Enhancement of dampinglike spin-orbit torque efficiency using light and heavy nonmagnetic metals on a polycrystalline RuO₂ layer

Yoshiaki Saito ,^{1,*} Shoji Ikeda ,^{1,2,3} Shutaro Karube,⁴ and Tetsuo Endoh ,^{1,2,3,5}

¹Center for Innovative Integrated Electronic Systems, Tohoku University, Sendai 980-8572, Japan

²Center for Science and Innovation in Spintronics, Tohoku University, Sendai 980-8577, Japan

³Research Institute of Electrical Communication, Tohoku University, Sendai 980-8577, Japan

⁴Institute for Chemical Research, Kyoto University, Kyoto 611-0011, Japan

⁵Department of Electrical Engineering, Graduate School of Engineering, Tohoku University, Sendai 980-8579, Japan

(Received 20 May 2024; revised 17 September 2024; accepted 25 September 2024; published 15 October 2024)

Crystal growth and magnetic and spin-orbit torque (SOT) properties of the systems with polycrystalline RuO_2 consisting of $RuO_2/SHM/Co/Ir/MgO/Ta$ (SHM = Pt, [Pt/Ir] multilayer) and $RuO_2/NM/Pt/Co/Ir/MgO/Ta$ (NM = Ru, Ti) and the effects of RuO_2 and light or heavy metal (NM and SHM) interfaces on spin current generated from the spin-split band (SSB) are investigated. The Pt layer and [Pt/Ir] multilayer on the polycrystalline RuO_2 layer have flat and (111) texture, which induces perpendicular magnetization of Co. Enhancement of dampinglike SOT efficiency (ξ_{DL}) in the thin Pt and [Pt/Ir]-multilayer thickness region and nearly constant magnitude of ξ_{DL} as a function of the thickness of NM = Ti are observed. Moreover, field-free switching was observed even in the polycrystalline RuO_2/Pt heavy metal system in the thin Pt thickness region ($t_{Pt} \le 2$ nm). The observed field-free switching may be related to the exchange bias from the antiferromagnetic RuO_2 layer to the Co layer through a thin Pt layer. The spin-torque ferromagnetic resonance results show that the x- and z-spin polarizations originating from SSB are canceled out for the polycrystalline RuO_2 system. These results indicate that the efficiency of SOT is enhanced by orbital Rashba-Edelstein, spin Hall, and orbital Hall effects. We expect that polycrystalline RuO_2 -based systems will pave the way to antiferromagnetic spintronics.

DOI: 10.1103/PhysRevB.110.134423

I. INTRODUCTION

The recently discovered phenomenon of spin-split bands in compensated collinear symmetry antiferromagnets, called altermagnetism [1–8], has attracted a great deal of attention. RuO₂ is a typical altermagnet [1–8] and has attractive properties such as low resistivity, thermal resistance, chemical stability, and so on [9-11]. RuO₂ is an antiferromagnetic material up to room temperature and the Néel vector aligns along the [001] axis [2]. A recent theoretical paper has shown that an anisotropic spin-split band exists in collinear antiferromagnetic RuO2 and that spin current is generated from the spin-split band [4]. This spin current could be utilized to switch the magnetization of an adjacent ferromagnetic layer by the induced spin-orbit torque (SOT) and applications in spintronics devices such as SOT magnetic random-access memory (MRAM) and spin-based logic devices have been expected [12–32]. Recent experiments in RuO₂ [4,5,8] have shown that the SOT from the spin-split band [spin-split effect (SSE)] is an anisotropic phenomenon and that the crystal growth orientation must be controlled and the direction of current flow must be carefully selected to achieve field-free SOT switching. Because a (101) texture for the crystal growth of RuO₂ film and a current flowing along the [010]-direction of RuO₂ film are needed for the field-free switching of the system, single crystal substrates such as Al₂O₃ and TiO₂ are

In this study, we conducted systematic experiments aiming to understand the crystal growth and SOT property of RuO_2 on SiO_2 substrates and the effects of RuO_2 and light or heavy metal interfaces on spin current generated from the spin-split band. As a result, using the heavy metal of Pt and [Pt/Ir] multilayer as a material on RuO_2 , we observed enhancement of the efficiency of SOT and perpendicular magnetization of a Co layer adjacent to the Pt and [Pt/Ir] multilayer, as well as field-free switching in the polycrystalline RuO_2 /Pt heavy metal system with the Pt thickness of $t_{Pt} \leq 2$ nm.

II. EXPERIMENTAL PROCEDURE

We fabricated the systems consisting of RuO₂/Pt/Co/Ir/MgO/Ta (samples A and E),

usually used for the crystal growth of RuO_2 film [4,5,8]. However, in general, memory devices for a large-scale integration (LSI) must be fabricated on Si or SiO_2 , making it difficult to control the growth orientation and select the crystal direction for current flow. In addition to these limitations, the use of only the RuO_2 is insufficient to achieve highly efficient current to spin conversion [5,8]. The efficiency of current to spin conversion, that is, dampinglike SOT efficiency (ξ_{DL}) in the RuO_2 , is less than 10% [5,8]. On the other hand, recently it has been reported that oxygen treatment of light elements has a strong effect on the orbital Hall effect (OHE) [33–39] and spin Hall effect (SHE) [40], and enhancement of SOT has been observed due to the orbital Rashba-Edelstein effect (OREE).

^{*}Contact author: yoshiaki.saito.d7@tohoku.ac.jp

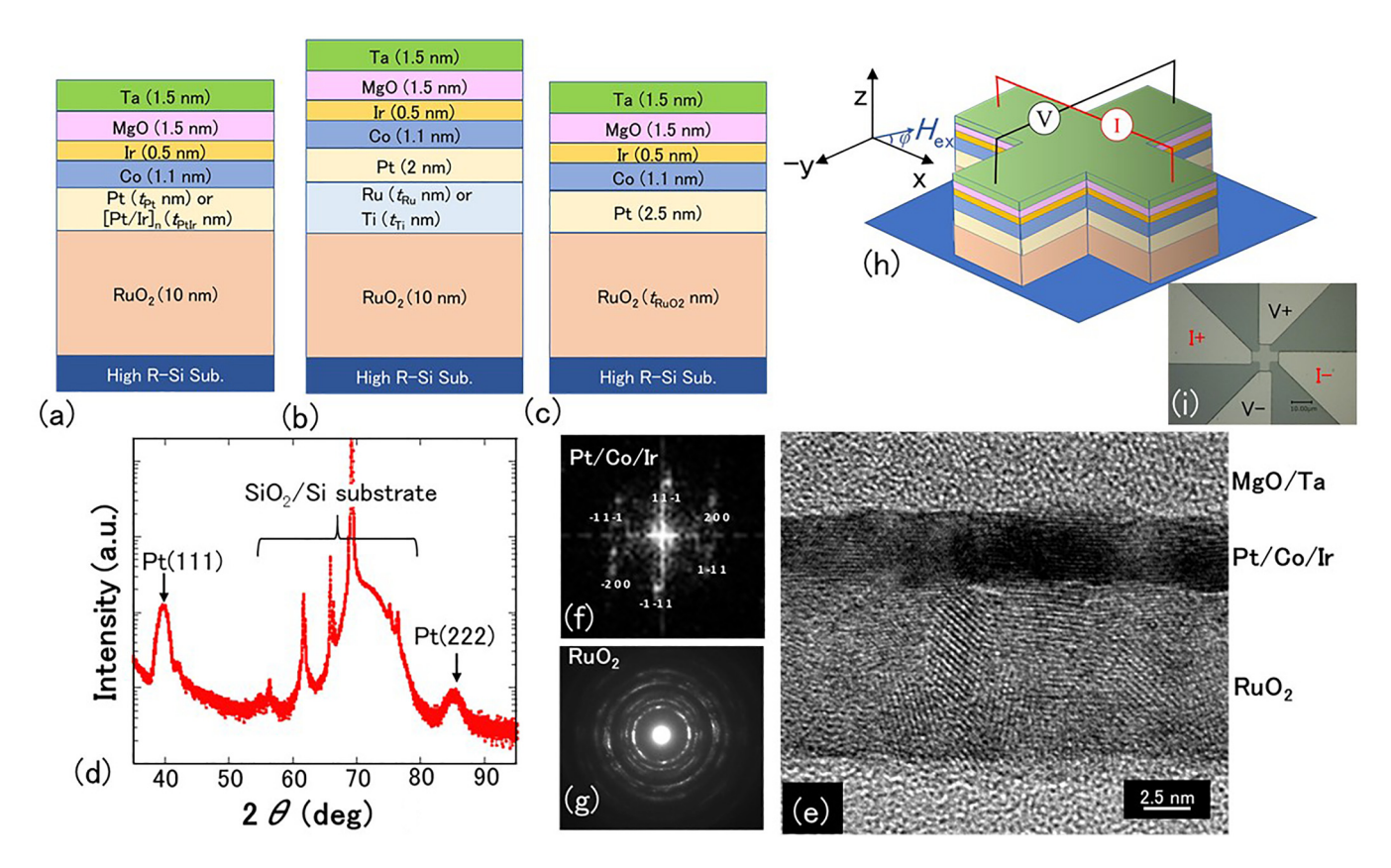


FIG. 1. (a–c) Schematic of prepared film structures for samples A–E in Table I. (d) Result of x-ray diffraction (XRD) measurement for sample A. (e) Cross-sectional transmission electron microscopy image in sample A and (f,g) the results of transmission electron diffraction of Pt/Co/Ir and Pt/Co/Ir

RuO₂/[Pt/Ir]-multilayer/Co/Ir/MgO/Ta (sample B), RuO₂/Ru/Pt/Co/Ir/MgO/Ta (sample C), and RuO₂/Ti/Pt/Co/Ir/MgO/Ta (sample D) as shown in Figs. 1(a)–1(c). In order to confirm the existence of the z component of spin current or not, we also fabricated the sample of RuO₂(10)/Pt(2)/Ni₈₁Fe₁₉(5)/Ir(0.5)/MgO(1.5)/Ta(1.5) (sample F) for spin-torque ferromagnetic resonance (ST-FMR) measurement, where the numbers in the parentheses show the nominal thickness in nanometers. All stack structures in this study are prepared on thermal

oxidized Si (SiO₂) substrates by rf sputtering on rotating substrates. Detailed film structures of samples A–D are shown in Table I. The RuO₂ films were grown by reactive sputtering at 573 K in a mixture of argon (70%) and oxygen (30%) gases. The base pressure during the deposition of the RuO₂ films was 3×10^{-6} Pa and the reactive pressure was 0.13 Pa with a power of 150 W [41]. Then, after the films were cooled down to room temperature, other layers were deposited at room temperature. As shown in Table I, from here the prepared samples are called "sample A"—"sample F."

TABLE I. Detailed sample structure (stack) prepared in this study, magnetic easy axis of ferromagnetic layers, and maximum magnitude of dampinglike SOT efficiency (ξ_{DL}).

Sample name	Structure of prepared films	Thickness (nm)	Easy-axis direction of ferromagnet	Maximum ξ _{DL} (%)
A	$RuO_2(10)/Pt(t_{Pt})/Co(1.1)/Ir(0.5)/MgO(1.5)/Ta(1.5)$	$t_{\text{Pt}} = 1.5, 2.0, 2.5,$ 3.0, 4.0, 5.0	Out of plane	28.3
В	$RuO_2(10)/[Pt(1.0)/Ir(0.8)]_n/Co(1.1)/Ir(0.5)/MgO(1.5)/Ta(1.5)$	$t_{\text{PtIr}} = 1.8, 2.8, 3.6,$ 4.6, 5.4	Out of plane	27.1
С	$RuO_2(10)/Ru(t_{Ru})/Pt(2)/Co(1.1)/Ir(0.5)/MgO(1.5)/Ta(1.5)$	$t_{\text{Ru}} = 1.0, 2.0, 3.0,$ 4.0, 5.0	Out of plane	22.5
D	$RuO_2(10)/Ti(t_{Ti})/Pt(2)/Co(1.1)/Ir(0.5)/MgO(1.5)/Ta(1.5)$	$t_{\text{Ti}} = 1.0, 2.0, 3.0,$ 4.0, 5.0	Out of plane	26.1
E	$RuO_2(t_{RuO2})/Pt(2.5)/Co(1.1)/Ir(0.5)/MgO(1.5)/Ta(1.5)$	$t_{\text{RuO}_2} = 5.0, 7.0,$ 9.0, 11.0, 13.0, 15.0	Out of plane	26.3

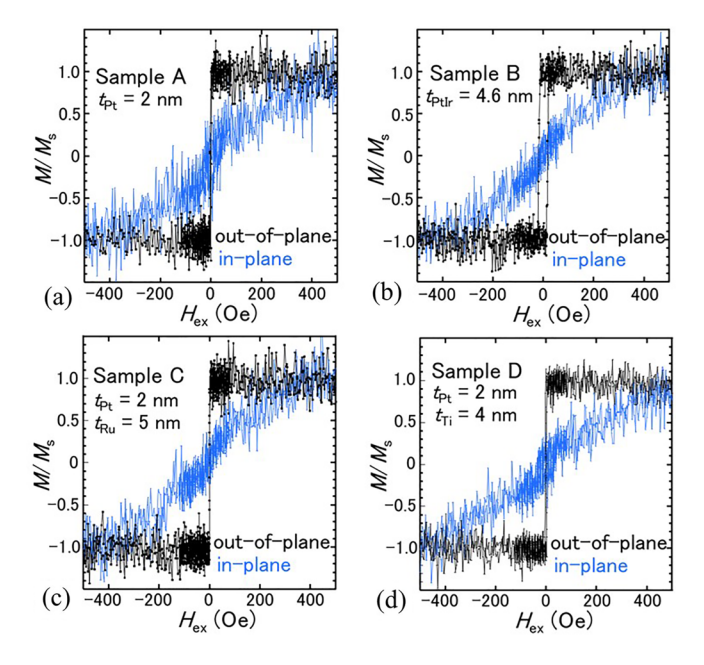


FIG. 2. (a–d) Normalized out of plane and in-plane magnetization vs field (*M-H*) curves for samples A–D in Table I, respectively. All films have perpendicular magnetic anisotropy.

A typical cross-sectional transmission electron microscope (TEM) image and the typical result of x-ray diffraction (XRD) measurement using a standard Cu anode x-ray tube for sample A are shown in Figs. 1(d) and 1(e), respectively. Results of the transmission electron diffraction (TED) patterns for Pt/Co/Ir and RuO₂ films are also shown in Figs. 1(f) and 1(g), respectively. The TEM image of Fig. 1(e) and the TED pattern shown in Fig. 1(g) indicate that RuO2 film is polycrystalline with a grain size of about 4 nm for the 10 nm thick RuO₂ film ($t_{RuO_2} = 10 \text{ nm}$). Although Pt film generally tends to grow granularly [42] on an oxidized substrate, thanks to the polycrystalline RuO2 underlayer, Pt film on RuO2 film was found to be flat and has a face centered cubic (fcc) structure with the (111) texture [Figs. 1(d) and 1(g)]. The TEM images also show that the top Ta is oxidized. These XRD and TEM results are consistent with each other. Detailed XRD patterns in samples A-D are shown in the Supplemental Material, Note 1 [43]. In the samples inserting the nonmagnetic layers of Ru or Ti between Pt and RuO₂ films (samples C and D), the peaks of the out of plane XRD θ -2 θ diffraction patterns have small intensities and broad width compared to those for samples A and B as shown in the Supplemental Material, Note 1 [43]; however, the peaks still exist at around fcc Pt (111) and fcc Ir (111). The device fabrications shown in Figs. 1(h) and 1(i) are done in a similar way to that in Ref. [44]. The magnetization measurements were carried out by a vibrating sample magnetometer (VSM). The anomalous Hall effect (AHE) and current-induced magnetization SOT switching were measured by the four-point probe method in a Hall cross at room temperature. The measurement configuration is sketched in Fig. 1(h). By rotating the samples, the external magnetic field was applied in any direction in the z-x plane to estimate the ξ_{DL} . Considering magnetization saturation and magnetization hysteresis, we have measured data for both clockwise and counterclockwise rotations for the round trips of $-30^{\circ} \rightarrow +280^{\circ} \rightarrow -30^{\circ}$ with the angle controlled every 0.2° at various magnitudes of the external magnetic field. For measuring ST-FMR, the films were patterned into rectangular microstrips with a width of 10 µm and length of 20 µm, using photolithography and ion milling techniques. Subsequently, the ground-signal-ground (G-S-G) coplanar waveguide (CPW) electrodes were fabricated by photolithography, sputtering, and lift-off techniques. An rf current with frequencies from 7 to 12 GHz was applied by a signal generator. This generator was connected to the rf port of the bias tee, and the rf signal was conveyed to the ST-FMR device through an rf cable and G-S-G probe. The ST-FMR signal is simultaneously detected by a lock-in amplifier which was connected to the low-frequency port of the bias tee via the spin rectification effect driven by anisotropic magnetoresistance. Furthermore, we investigated the in-plane field-angular dependence of the signals to elucidate all x-, y-, and z-polarized spin components of the generated spin current.

III. RESULTS OF MAGNETIC AND ELECTRICAL PROPERTIES

A. Magnetic properties

Figures 2(a)-2(d) show the typical normalized out of plane and in-plane magnetization versus field (M-H) curves for samples A—D with $t_{Co} = 1.1$ nm, respectively. The M-H curves indicate that Co films on Pt and [Pt/Ir] multilayer in samples A-D have perpendicular magnetization, because Pt/Co/Ir films have a flat and fcc (111) texture as shown in Figs. 1(d) and 1(f). Corresponding AHE curves for samples A-D are shown in the Supplemental Material, Note 2 [43]. The Hall resistivity is expressed [45,46] by $\rho_H = R_0 H_{\rm ex} + 4\pi R_{\rm s} M_{\rm z} \propto$ R_{xy} , where $R_0H_{\rm ex}$, $4\pi R_sM_z$ are terms of ordinal and anomalous Hall effects, when applying an external magnetic field $(H_{\rm ex})$. $R_{\rm xv}$, $R_{\rm s}$, and $M_{\rm z}$ are the anomalous Hall resistance, a constant that characterizes the strength of the anomalous Hall resistance, and the corresponding z-axis component of magnetization of the Co layer, respectively. The results of the AHE curves show hysteresis loops with a good square shape and are consistent with those of the M-H curves shown in Figs. 2(a)— 2(d). These results are good for memory application because the use of devices with perpendicular magnetic anisotropy (PMA) [47] is essential for achieving high-density memory.

B. Estimation of spin-orbit torque efficiency ξ_{DL}

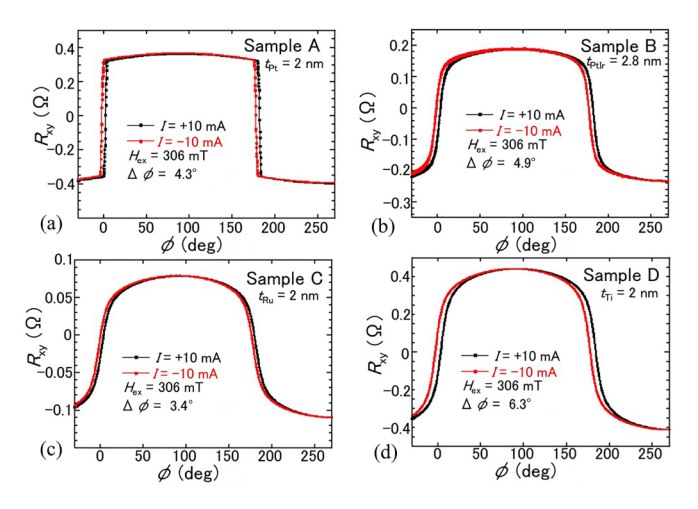


FIG. 3. Anomalous Hall curves measured when rotating an external magnetic field of 306 mT in the *z-x* plane of Fig. 1(h) with current $I=\pm 10\,\mathrm{mA}$ for (a) sample A ($t_\mathrm{Pt}=2\,\mathrm{nm}$), (b) sample B ($t_\mathrm{PtIr}=2.8\,\mathrm{nm}$), (c) sample C ($t_\mathrm{Ru}=2.0\,\mathrm{nm}$, $t_\mathrm{Pt}=2.5\,\mathrm{nm}$), and (d) sample D ($t_\mathrm{Ti}=2.0\,\mathrm{nm}$, $t_\mathrm{Pt}=2.5\,\mathrm{nm}$).

the resistivity of the RuO₂ layer is slightly smaller than that of the conductive Ti layer, indicating that the RuO₂ layer can be used as wiring for SOT-MRAM thanks to its low resistivity.

Figures 3(a)–3(d) show the typical R_{xy} versus φ curves between $-30^{\circ} \leqslant \varphi \leqslant 280^{\circ}$ for samples A $(t_{Pt} = 2 \text{ nm})$, B $(t_{\text{PtIr}} = 2.8 \text{ nm})$, C $(t_{\text{Ru}} = 2 \text{ nm})$, and D $(t_{\text{Ti}} = 2 \text{ nm})$, respectively. These curves are measured at $H_{\rm ex} = 306 \, \rm mT$ and I = ± 10 mA. As shown in Figs. 3(a)–3(d), switching is observed at around $\varphi = 0^{\circ}$ and $\varphi = 180^{\circ}$ for all samples. Because the magnetization switching occurs by a combination of the z component of the external magnetic field and the SOT effect, the opposite horizontal angle shift $(\Delta \varphi)$ for the positive and negative current in the R_{xy} versus φ curves is observed as shown in Figs. 3(a)-3(d). The magnitudes of the shift of angle $\Delta \varphi$ are 4.3°, 4.9°, 3.4°, and 6.3° for samples A–D at $H_{\rm ex}$ 306 mT, respectively. The values of $\Delta \varphi$ were estimated from the difference in the center of the magnetization coercive force obtained from both clockwise and counterclockwise rotation data when the current was applied in the +I and -I directions. When the rotating angle φ is small, the z component of the magnetic field $H_z = H_{\rm ex} \sin \varphi \approx \varphi H_{\rm ex}$, so, the SOT effective magnetic field $(H_{\rm eff})$ is estimated using $H_{\rm eff} = H_{\rm ex} \Delta \varphi$ [48].

Figures 4(a)–4(d) show the efficiency of effective field $\chi = H_{\rm eff}/J$ as a function of $H_{\rm ex}$ for samples A–D, where J is a current density during measurement. Here we used the magnitude of the current density of the Pt or [Pt/Ir] multilayer for the magnitude of J, where the amount of current flowing through each layer is estimated as proportional to the inverse of the resistance, which depends on the thickness of each layer and the magnitude of the estimated resistivity (Supplemental Material, Note 3 [43]).

The magnitude of χ is related to the ξ_{DL} [30–32,48],

$$\xi_{\rm DL} = \frac{8\chi e\mu_0 M_s t}{h\cos(\beta)},\tag{1}$$

where e, t, h, μ_0, M_s , and t are elementary charge, thickness of the ferromagnetic layer, Planck constant, permeability of

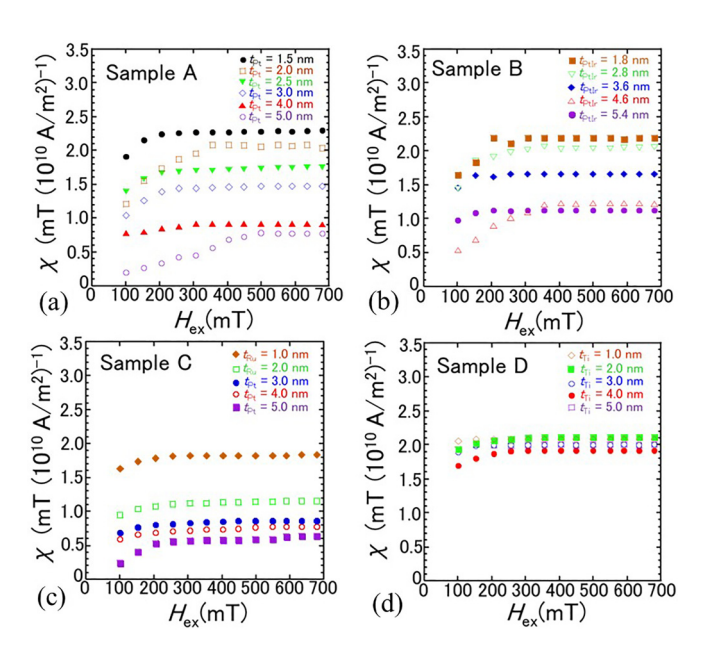


FIG. 4. Efficiency of effective field $\chi = H_{\rm eff}/J$ as a function of the $H_{\rm ex}$ for (a) samples A, (b) samples B, (c) samples C, and (d) samples D for various thicknesses of $t_{\rm Pt}$, $t_{\rm Pulr}$, $t_{\rm Ru}$, and $t_{\rm Ti}$.

vacuum, saturation magnetization of Co, and thickness of Co layer, respectively. The $cos(\beta)$ value is equal to 1 in the high $H_{\rm ex}$ region, because the angle (β) between the current direction and the central moment direction of the domain wall in a Co layer [48] would be parallel in the high $H_{\rm ex}$ region. The values of $M_s t$ used to estimate the value of ξ_{DL} are almost the same for samples A–D, $0.66 \pm 0.03 \times 10^{-3}$ A, and are obtained from the VSM measurement. Therefore, we used the magnitude of $M_s t = 0.66 \times 10^{-3}$ A for the estimation of ξ_{DL} . As shown in Figs 4(a)-4(d), the magnitude of χ increases with increasing $H_{\rm ex}$ and saturates at around $H_{\rm ex} \approx 300 \sim 500\,{\rm mT}$. These results are consistent with previous reports [30,48]. The saturation behavior of χ indicates that the angle (β) between the central moment direction of the domain wall and the current direction becomes zero in the high $H_{\rm ex}$ region as discussed in Refs. [30,48].

Figure 5(a) shows dependences of ξ_{DL} on t_{Pt} and t_{PtIr} for samples A and B, respectively. As shown in Fig. 5(a), the magnitudes of ξ_{DL} have a maximum when t_{Pt} and t_{PtIr} are

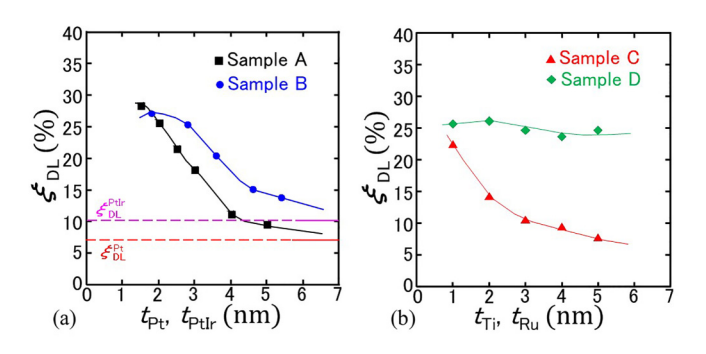


FIG. 5. Efficiency of spin torque [dampinglike SOT efficiency (ξ_{DL})] as functions of the t_{Pt} , t_{PtIr} for samples A and B (a), and t_{Ru} and t_{Ti} for samples C and D (b).

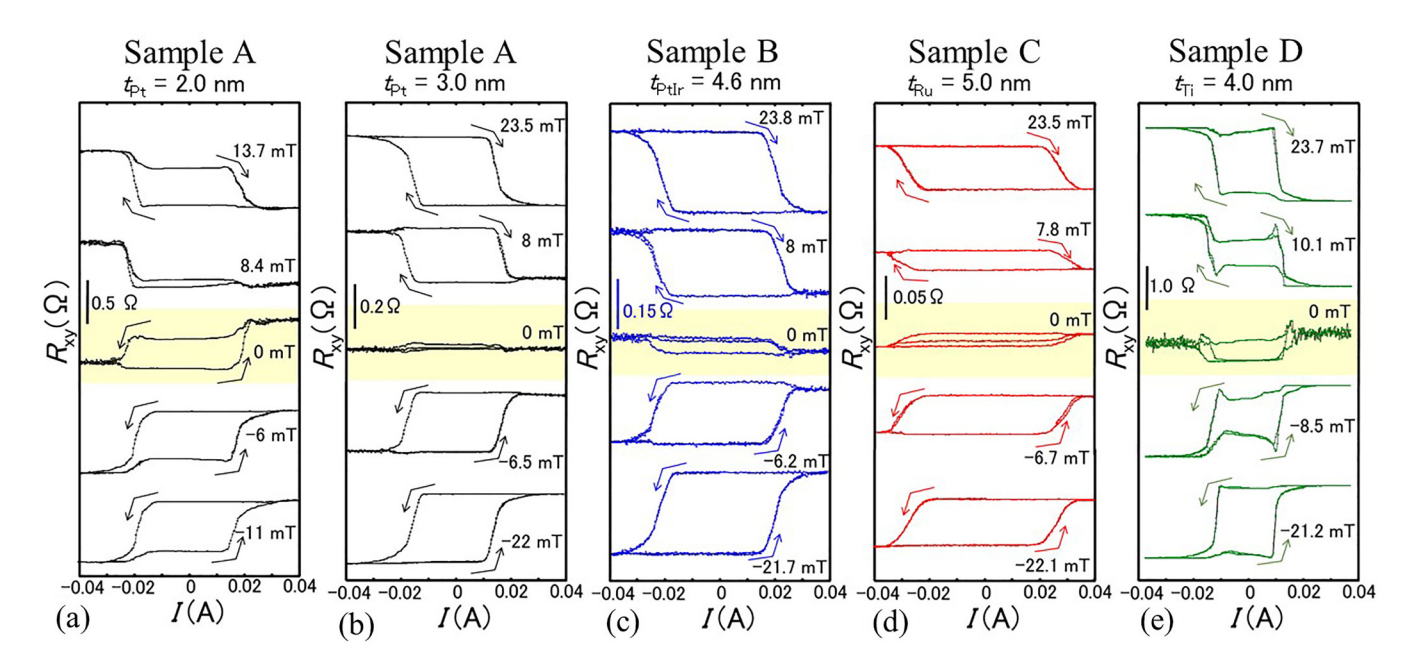


FIG. 6. Typical current-induced SOT switching for (a) sample A ($t_{Pt} = 2.0 \text{ nm}$), (b) sample A ($t_{Pt} = 3.0 \text{ nm}$), (c) sample B ($t_{PtIr} = 4.6 \text{ nm}$), (d) sample C ($t_{Ru} = 5.0 \text{ nm}$, $t_{Pt} = 2.5 \text{ nm}$), and (e) sample D ($t_{Ti} = 4.0 \text{ nm}$, $t_{Pt} = 2.5 \text{ nm}$). Field-free switching is observed in sample A ($t_{Pt} = 2.0 \text{ nm}$).

around 2 nm or below for samples A and B. In Fig. 5(a), we plotted the values of ξ_{DL} (= 7.0%, 10.3%) with red and pink dotted lines in Fig. 5(a) for the Pt heavy metal layer (7.2 nm) and the [Pt/Ir] heavy metal multilayer (7.2 nm), respectively, which were estimated by the same measurement method as in our previous study [30]. The maximum magnitude of ξ_{DL} in samples A and B shown in Fig. 5(a) is much larger than those in the Pt layer [30,49–52], [Pt/Ir] multilayer [30], and RuO₂ layer [5,8]. The ratio of ξ_{DL} (samples A and B)/ ξ_{DL} (Pt layer) increases by a factor of 4 or more. Increasing the t_{Pt} and t_{PtIr} , the magnitudes of ξ_{DL} for samples A and B approach those of the Pt layer and [Pt/Ir] multilayer, respectively. These findings likely result from an orbital current generated at the interface between RuO₂ and Pt (OREE), which is injected into the Pt layer and the [Pt/Ir] multilayer and enhances the efficiency of SOT by strong spin-orbit coupling in the Pt layer and [Pt/Ir] multilayer. This trend of ξ_{DL} as a function of t_{Pt} is nearly consistent with previous results [40].

Figure 5(b) shows dependences of ξ_{DL} on t_{Ru} and t_{Ti} for samples C and D, respectively. Surprisingly, a nearly constant magnitude of ξ_{DL} as a function of t_{Ti} is observed for sample D, whereas a monotonous decrease of ξ_{DL} as a function of t_{Ru} is observed in sample C. This indicates that the amount of the spin current reaching Co decreases with t_{Ru} , whereas it does not change for t_{Ti} . This would be related to the recently observed large and long-range propagation of orbital currents in the Ti layer [53]. We would like to discuss later the physical origin of the SOT to the Co layer in these samples.

In the case of the RuO₂ thickness (t_{RuO_2}) dependence of ξ_{DL} (sample E), as shown in the Supplemental Material, Note 4 [43], the magnitude of the ξ_{DL} shows a slight maximum around $t_{RuO_2} = 7$ nm. The increase in dampinglike torque below 7 nm with increasing t_{RuO_2} indicates that the dampinglike torque is affected by the bulk effect and not only by the purely interfacial effect. The reason for the small dependence of

dampinglike torque on t_{RuO_2} is thought to be that the resistance of RuO2 is higher than that of the Pt layer, so the current flows more in the Pt layer, making it difficult to see the effect of increasing t_{RuO_2} . The slight decrease in ξ_{DL} thicker than $t_{RuO_2} > 7$ nm indicates that as long as the crystal quality of RuO_2 is maintained, it is presumed that the t_{RuO_2} should not be thicker than 7 nm because the amount of current that must flow in the RuO₂ layer would increase due to the increased current shunting to the RuO2 layer. Because Tint is given by $T_{\rm int} \leqslant 1$ [54–57], a lower limit of spin Hall angle ($\theta_{\rm SH}$) is given by $\theta_{\rm SH} = \xi_{\rm DL}/T_{\rm int} \geqslant \xi_{\rm DL} \sim \xi_{\rm DL}$, assuming interfacial spin transparency $T_{\rm int} \sim 1$. We show the results of a lower limit of spin Hall conductivity ($\sigma_{SH} = \theta_{SH}/\rho_{xx}$) for samples A–D (the Supplemental Material, Note 5 [43]), where ρ_{xx} is the resistivity of the total stack of samples A-D. The maximum magnitude of σ_{SH} is $\sim 2.5 \times 10^5 \, \Omega^{-1} \, m^{-1}$ for samples A–C and $1.9 \times 10^5 \, \Omega^{-1} \, m^{-1}$ for sample D. The small magnitude of σ_{SH} in sample D is related to the large value of resistivity of Ti film (ρ_{Ti}) .

C. Current-induced spin-orbit torque switching

Next we show the typical current-induced SOT switching in Figs. 6(a)–6(e) for samples A ($t_{Pt} = 2.0 \,\mathrm{nm}$), A ($t_{Pt} = 3.0 \,\mathrm{nm}$), B ($t_{PtIr} = 4.6 \,\mathrm{nm}$), C ($t_{Ru} = 5.0 \,\mathrm{nm}$), and D ($t_{Ti} = 4.0 \,\mathrm{nm}$), respectively. For this experiment, R_{xy} is recorded during the scanning of a pulse current (I) applied to the x axis of the Hall bars shown in Fig. 1(h) with an external magnetic field along the $\pm x$ directions (H_x). The pulse current width used in Figs. 6(a)–6(e) is 200 μ s. As shown in Fig. 6(a), the current-induced SOT switching shows opposite polarities under $H_x > 8.4 \,\mathrm{mT}$ (clockwise switching direction) and $H_x < 8.4 \,\mathrm{mT}$ (anticlockwise switching direction) for sample A ($t_{Pt} = 2 \,\mathrm{nm}$); thus we observe field-free switching for sample A ($t_{Pt} = 2 \,\mathrm{nm}$). Comparing the magnitude of the SOT-

reversed R_{xy} at 0 mT with the magnitude of the R_{xy} at 0 mT when the H_{ex} is swept (see the Supplemental Material, Note 2 [43]), it is found that 65% of the volume of Co is SOT switched by applying the pulse current. Considering that 75% of the volume of Co could be SOT switched by controlling the crystal growth orientation to the (101) texture and the current direction to the [010] direction of the RuO₂ film [8], observed field-free switching for a relatively large amount of Co volume (65%) using polycrystalline RuO₂ is surprising. This result might indicate that theoretically predicted unconventional spin currents with x- and z-spin polarization via the spin-split band in antiferromagnets [3,4] exist even in polycrystalline RuO₂ through a thin Pt layer. However, xand z-spin polarization should be canceled out for complete polycrystalline samples. We would like to discuss later the reason for the observed field-free switching. The changes in the R_{xy} under $H_x = 0 \,\mathrm{mT}$, after applying 200 µs writing pulses of amplitude $I = \pm 35$ mA for sample A ($t_{Pt} = 2.0$ nm), are shown in the Supplemental Material, Note 6 [43]. The absolute values of the R_{xy} changes in the SOT switching are consistent with that in the SOT switching in Fig. 6(a); therefore, 65% of the volume of Co is SOT switched successfully and stably. On the other hand, when increasing the thickness of the Pt layer thicker than 2 nm, we could not observe field-free switching as shown in Fig. 6(b). In samples B-D, the current-induced SOT switching shows opposite polarities under $H_x > 0$ mT (clockwise switching direction) and $H_x < 0 \,\mathrm{mT}$ (anticlockwise switching direction) as shown in Figs. 6(c)-6(e). We observe small hysteresis loops at $H_x =$ 0 mT in the SOT switching as shown in Figs. 6(c)–6(e); however, their magnitudes of the R_{xy} were less than 20% of the volume of Co observed in the external magnetic field dependence (Supplemental Material, Note 2 [43]).

IV. DISCUSSION

We would like to discuss the physical origin of the SOT on the Co layer observed in samples A–D with a polycrystalline RuO₂ layer and possible reasons for field-free SOT switching in sample A in the thin t_{Pt} region. As shown in Fig. 5(a), we observed the enhancement of SOT efficiency in samples A and B compared to those of Pt, [Pt/Ir] multilayer and RuO₂ layers. The current to spin current conversion efficiency is enhanced and the ratio of ξ_{DL} (samples A and B)/ ξ_{DL} (Pt layer) increases by a factor of 4 or more in the thin t_{Pt} and t_{PtIr} regions as described before. These findings indicate that the orbital current generated at the interface between RuO2 and Pt (OREE) would be one of the origins of the spin conduction mechanism in our systems. Moreover, we also observe field-free SOT switching in sample A in the thin t_{Pt} region $(t_{\rm Pt} \le 2 \, \rm nm)$ as shown in Fig. 6(a). This result might indicate that unconventional spin currents with x- and z-spin polarization via the spin-split effect (SSE) in antiferromagnets [3,4] exist even in polycrystalline RuO2 through a thin Pt layer, and insertion of Pt between Co and RuO₂ could enhance the SOT originating from the SSE. However, x- and z-spin polarization should be canceled out for complete polycrystalline samples as discussed before.

To confirm the existence of x and z components of spin current, we measured ST-FMR in sample F (the Supplemental

Material, Note 7 [43]). As shown in the Supplemental Material, Note 7 [43], the observed ST-FMR signal $V_{\rm mix}$ [(Fig. S7(a)] as a function of the applied in-plane magnetic field (H) consists of the Lorentzian L and its derivative, $V_{\rm mix} = V_s L(H) + V_A \partial_H L(H)$ [58,59], where V_s and V_A correspond to the amplitudes of Lorentzian and its derivative, respectively. We summarized the amplitudes as a function of the applied field angle (ϕ_H) (Fig. S7(b) in the Supplemental Material, Note 7 [43]). The dampinglike (DL) and fieldlike (FL) torques of x-, y-, and z-polarized spin currents can be separated from the ϕ_H dependence using Eqs. (2)–(5) [60,61].

$$V_{\mathcal{S}}(\phi_H) = \sin 2\phi_H \left[V_{\mathcal{S}}^x \sin \phi_H + V_{\mathcal{S}}^y \cos \phi_H + V_{\mathcal{S}}^z \right]$$
 (2)

$$\propto \sin 2\phi_H \left[h_{\rm DL}^x \sin \phi_H + h_{\rm DL}^y \cos \phi_H + h_{\rm FL}^z \right], \quad (3)$$

$$V_A(\phi_H) = \sin 2\phi_H \left[V_A^x \sin \phi_H + V_A^y \cos \phi_H + V_A^z \right]$$
 (4)

$$\propto \sin 2\phi_H \left[h_{\rm FL}^x \sin \phi_H + h_{\rm FL}^y \cos \phi_H + h_{\rm DL}^z \right].$$
 (5)

Here h_{DL}^{i} and h_{FL}^{i} represent the amplitudes of the DL torque and FL torque, respectively; i = x, y, z spin polarization components. As shown in Fig. S7(b) in the Supplemental Material, Note 7 [43], the fitting was successful. We obtain the values of $V_S^x = -0.9 \,\mu\text{V}$, $V_S^y = -64.6 \,\mu\text{V}$, $V_S^z = -0.5 \,\mu\text{V}$, $V_A^x = -1.5 \,\mu\text{V}$, $V_A^y = -103 \,\mu\text{V}$, and $V_A^z = -0.9 \,\mu\text{V}$. Because the magnitudes of V_S^x (V_A^x) and V_A^z (V_S^z) are negligibly small compared to those of V_S^y (V_A^y), both DL and FL spin-orbit fields have a dominant y component, and unconventional spin currents with x- and z-spin polarization via the SSE in antiferromagnets are negligibly small. This result indicates that x- and z-spin polarizations are canceled out for the polycrystalline samples and only ordinal y-spin polarization exists in the polycrystalline RuO₂/Pt system. Considering this ST-FMR result, the observation of field-free switching would come from other effects, such as the tilting of the easy axis of PMA. Interfacial Dzyaloshinskii-Moriya (DM) interaction [62,63] would be one of the possible reasons for the tilting of the easy axis of PMA. Sample A has the Pt/Co/Ir interfaces. The magnitude of the interfacial DMI is small for the Pt/Co/Ir structure, because the DMI at the interface of Co and Ir is similar in magnitude to that of the Co and Pt, and the Pt/Co interface and Co/Ir interface possess the opposite sign [32]. However, because the RuO₂/Pt/Co/Ir system has a small coercivity as shown in Figs. 2(a) and S2(a) in the Supplemental Material, Note 2 [43], the easy axis of PMA in this system would be easily tilted. In fact, we also observe small hysteresis loops at $H_x = 0$ mT in the SOT switching for other samples with Pt/Co/Ir interfaces as discussed previously and shown in Figs. 6(c)-6(e). Another possible reason would be the exchange bias from the antiferromagnetic RuO₂ layer to the Co layer through the thin Pt layer ($t_{Pt} \leq 2 \text{ nm}$). To confirm the existence of the bias field, we measured the AHE curve sweeping H_{ex} in the x direction in Fig. 1(h) (Supplemental Material, Note 8 [43]). As a result, we observed the bias field shift of $\Delta H = 11.6$ mT as shown in the Supplemental Material, Note 8 [43]. This bias field shift would be the reason for the observed field-free switching in sample A. We think that the observed bias shift would be related to the exchange bias from the antiferromagnetic RuO₂ layer to the Co layer through a thin Pt layer ($t_{Pt} \leq 2 \text{ nm}$); however, we did not perform postannealing in an external magnetic field as in the previous

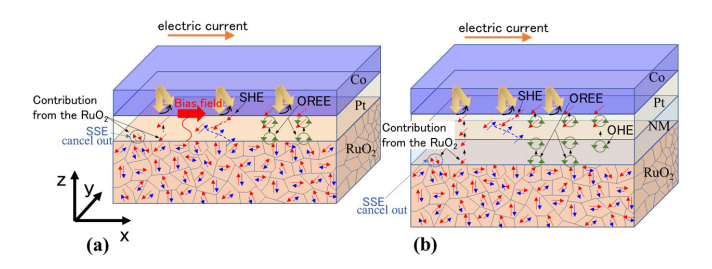


FIG. 7. Schematic diagrams of the model for explaining the experimental results observed in (a) samples A, B, and E and (b) samples C and D.

study [64]. We should make more efforts to understand the details for observed field-free switching even in the polycrystalline RuO_2/Pt heavy metal system in the thin Pt thickness region ($t_{Pt} \leq 2 \text{ nm}$).

Figures 7(a) and 7(b) show the schematic diagrams of our claim for explaining the experimental results observed in sample A and samples C and D (in the case of inserting the nonmagnetic metal (NM = Ru, Ti) between Pt and RuO₂. layers), respectively. As shown in Fig. 7(a), in addition to the OREE, the spin Hall effect (SHE) in the Pt layer should also exist in sample A. As discussed in the ST-FMR result (Supplemental Material, Note 7 [43]), the x- and z-spin polarizations originated from SSE are canceled out for the polycrystalline sample and only ordinal y-spin polarization exists. In terms of the y-spin polarization, it is not clear that this component comes from the SSE and/or SHE; however, there is a y-spin polarization component from the RuO₂ layer, because we observed the t_{RuO_2} dependence of ξ_{DL} as shown in the Supplemental Material, Note 4 [43]. We think that increasing the t_{Pt} would increase the ordinal spin torque (spin current with y-spin polarization via the SHE) from the Pt layer, which would decrease the effect of OREE in the thicker t_{Pt} region. In fact, we observed a maximum in the magnitudes of ξ_{DL} when t_{Pt} and t_{PtIr} were at around 2 nm or below for samples A and B. We also observed a bias field from the antiferromagnetic RuO₂ layer to the Co layer through a thin Pt layer ($t_{Pt} \leq 2 \text{ nm}$) as discussed before. In the case of inserting the NM between Pt and RuO₂ layers, the orbitals in interfacial RuO₂ might hybridize with those in the Ru or Ti insertion layer, which would contribute to the OREE. Moreover, in addition to the OREE and SHE, the orbital Hall effect (OHE) in the NM layer should contribute to the SOT on the Co layer. The observed nearly constant magnitude of ξ_{DL} as a function of t_{Ti} would be correlated to the long orbital current diffusion length recently observed in the Ni/Ti system [53].

As shown before, we have observed enhancement of ξ_{DL} in the thin Pt and [Pt/Ir]-multilayer thickness region. Recent reports [56,65–68] have shown that various heavy metals having Pt-based alloys such as Pt_{0.75}Au_{0.25}, Pt_{0.75}Pd_{0.25}, Pt_{0.57}Cu_{0.43}, Pt_{0.85}Hf_{0.15}, Pt_{0.8}Al_{0.2}, and Pt_{0.69}Cr_{0.31} show much improved SOT efficiency. Because these Pt alloys have an fcc structure, the same structure of Pt suggests that the topological characteristics of the Fermi surface of Pt and Pt alloys are nearly the same. This indicates that Pt-based alloys might also enhance the SOT. This would be an interesting topic for observation of more efficient SOT systems with polycrystalline RuO₂.

V. SUMMARY

In summary, we have studied the crystal growth and magnetic and SOT properties of the systems with RuO₂ on SiO₂ substrates consisting of RuO₂/SHM/Co/Ir/MgO/Ta (SHM = Pt, [Pt/Ir] multilayer), and RuO₂/NM/Pt/Co/Ir/MgO/Ta (NM = Ru, Ti) and the effects of RuO_2 and light or heavy metal (NM and SHM) interfaces on spin current generated from the spin-split band (SSB). The RuO₂ on the SiO₂ substrate was found to be polycrystalline, whereas the Pt layer and [Pt/Ir]-multilayer on the polycrystalline RuO2 layer have flat and (111)-texture, which induces perpendicular magnetization of Co. We also observed enhancement of ξ_{DL} in the thin $t_{\rm Pt}$ and $t_{\rm PtIr}$ regions and nearly constant magnitude of $\xi_{\rm DL}$ as a function of t_{Ti} . Moreover, field-free switching was observed even in the polycrystalline RuO₂/Pt heavy metal system with thin t_{Pt} ($t_{Pt} \le 2$ nm), which would be related to the exchange bias from the antiferromagnetic RuO₂ layer to the Co layer through a thin Pt layer. The ST-FMR results show that the xand z-spin polarizations originating from SSE are canceled out for the polycrystalline RuO₂ system. These results indicate that the efficiency of SOT is enhanced by OREE, SHE, and OHE. The results we observed here would advance magnetic memory devices with high density, high speed, and low power consumption. We expect that polycrystalline RuO2-based systems will pave the way to antiferromagnetic spintronics.

ACKNOWLEDGMENTS

This work was supported by the CIES Consortium, Ministry of Education, Culture, Sports, Science and Technology (MEXT) Initiative to Establish Next-Generation Novel Integrated Circuits Centers (X-NICS) through Grant No. JPJ011438, and Japan Society for the Promotion of Science (JSPS) KAKENHI (Grants No. JP24H00030 and No. JP21K18189). The authors also thank Tadamichi Miyazaki for TEM and TED observations.

^[1] Y. Sun, Y. Zhang, C-X. Liu, C. Felser, and B. Yan, Dirac nodal lines and induced spin Hall effect in metallic rutile oxides, Phys. Rev. B 95, 235104 (2017).

^[2] T. Berlijn, P. C. Snijders, O. Delaire, H.-D. Zhou, T. A. Maier, H.-B. Cao, S.-X. Chi, M. Matsuda, Y. Wang, M. R. Koehler, P. R. C. Kent, and H. H. Weitering, Itinerant antiferromagnetism in RuO₂, Phys. Rev. Lett. 118, 077201 (2017).

^[3] R. González-Hernáldez, L. Smejkal, Karel Vyborny, Y. Yahagi, J. Sinova, T. Jungwirth, and J. Zelezny, Efficient electrical spin

splitter based on nonrelativistic collinear antiferromagnetism, Phys. Rev. Lett. **126**, 127701 (2021).

^[4] A. Bose, N. J. Schreiber, R. Jain, D-F. Shao, H. P. Nair, J. Sun, X. S. Zhang, D. A. Muller, E. Y. Tsymbal, D. G. Schlom, and D. C. Ralph, Tilted spin current generated by the collinear antiferromagnet ruthenium dioxide, Nat. Electron. 5, 267 (2022).

^[5] H. Bai, L. Han, X. Y. Feng, Y. J. Zhou, R. X. Su, Q. Wang, L. Y. Liao, W. X. Zhu, X. Z. Chen, F. Pan, X. L. Fan, and

- C. Song, Observation of spin splitting torque in a collinear antiferromagnet RuO₂, Phys. Rev. Lett. **128**, 197202 (2022).
- [6] L. Šmejkal, J. Sinova, and T. Jungwirth, Beyond conventional ferromagnetism and antiferromagnetism: A phase with nonrelativistic spin and crystal rotation symmetry, Phys. Rev. X 12, 031042 (2022).
- [7] I. Mazin, Editorial: Altermagnetism—a new punch line of fundamental magnetism, Phys. Rev. X 12, 040002 (2022).
- [8] S. Karube, T. Tanaka, D. Sugawara, N. Kadoguchi, M. Kohda, and J. Nitta, Observation of spin-splitter torque in collinear antiferromagnetic RuO₂, Phys. Rev. Lett. 129, 137201 (2022).
- [9] H. Over, Surface chemistry of ruthenium dioxide in heterogeneous catalysis and electrocatalysis: From fundamental to applied research, Chem. Rev. 112, 3356 (2012).
- [10] M. Tamborin, S. Piccinini, M. Prudenziati, and B. Morten, Piezoresistive properties of RuO₂-based thick-film resistors: The effect of RuO₂ grain size, Sens. Actuators, A 58, 159 (1997).
- [11] A. Kirihara, M. Ishida, R. Yuge, K. Ihara, Y. Iwasaki, R. Sawada, H. Someya, R. Iguchi, K. Uchida, and E. Saito, Annealing-temperature-dependent voltage-sign reversal in alloxide spin Seebeck devices using RuO₂, J. Phys. D: Appl. Phys. 51, 154002 (2018).
- [12] L. Liu, C.-F. Pai, Y. Li, H. W. Tseng, D. C. Ralph, and R. A. Buhrman, Spin-torque switching with the giant spin Hall effect of tantalum, Science 336, 555 (2012).
- [13] G. Yu, P. Upadhyaya, Y. Fan, J. G. Alzate, W. Jiang, K. L. Wong, S. Takei, S. A. Bender, L.-T. Chang, Y. Jiang, M. Lang, J. Tang, Y. Wang, Y. Tserkovnyak, P. K. Amiri, and K. L. Wang, Switching of perpendicular magnetization by spin-orbit torques in the absence of external magnetic fields, Nat. Nanotechnol. 9, 548 (2014).
- [14] W. Jiang, P. Upadhyaya, W. Zhang, G. Yu, M. B. Jungfleisch, F. Y. Fradin, J. E. Pearson, Y. Tserkovnyak, K. L. Wang, O. Heinonen, S. G. E. Velthuis, and A. Hoffmann, Blowing magnetic skyrmion bubbles, Science 349, 283 (2015).
- [15] P. P. J. Haazen, E. Mure, J. H. Franken, R. Lavrijsen, H. J. M. Swagten, and B. Koopmans, Domain wall depinning governed by the spin Hall effect, Nat. Mater. 12, 299 (2013).
- [16] A. Chernyshov, M. Overby, X. Liu, J. K. Furdyna, Y. Lyanda-Geller, and L. P. Rokhinson, Evidence for reversible control of magnetization in a ferromagnetic material by means of spin-orbit magnetic field, Nat. Phys. 5, 656 (2009).
- [17] I. M. Miron, K. Garello, G. Gaudin, P.-J. Zermatten, M. V. Costache, S. Auffret, S. Bandiera, B. Rodmacq, A. Schuhl, and P. Gambardella, Perpendicular switching of a single ferromagnetic layer induced by in-plane current injection, Nature (London) 476, 189 (2011).
- [18] J. Kim, J. Sinha, M. Hayashi, M. Yamanouchi, S. Fukami, T. Suzuki, S. Mitani, and H. Ohno, Layer thickness dependence of the current-induced effective field vector in Ta|CoFeB|MgO, Nat. Mater. 12, 240 (2013).
- [19] S. Fukami, T. Anekawa, C. Zhang, and H. Ohno, A spin-orbit torque switching scheme with collinear magnetic easy axis and current configuration, Nat. Nanotechnol. 11, 621 (2016).
- [20] K.-S. Lee, S.-W. Lee, B.-C. Min, and K.-J. Lee, Thermally activated switching of perpendicular magnet by spin-orbit spin torque, Appl. Phys. Lett. **104**, 072413 (2014).
- [21] K. Garello, C. O. Avci, I. M. Miron, M. Baumgartner, A. Ghosh, S. Auffret, O. Boulle, G. Gaudin, and P. Gambardella, Ultrafast

- magnetization switching by spin-orbit torques, Appl. Phys. Lett. **105**, 212402 (2014).
- [22] C. Zhang, S. Fukami, H. Sato, F. Matsukura, and H. Ohno, Spin-orbit torque induced magnetization switching in nanoscale Ta/CoFeB/MgO, Appl. Phys. Lett. 107, 012401 (2015).
- [23] M. -H. Nguyen, C.-F. Pai, K. X. Nguyen, D. A. Muller, D. C. Ralph, and R. A. Buhrman, Enhancement of the anti-damping spin torque efficacy of platinum by interface modification, Appl. Phys. Lett. 106, 222402 (2015).
- [24] S. V. Aradhya, G. E. Rowlands, J. Oh, D. C. Ralph, and R. A. Buhrman, Plane magnetic tunnel junctions through dynamic Oersted-field-assisted spin Hall effect, Nano Lett. 16, 5987 (2016).
- [25] M. Baumgartner, K. Garello, J. Mendil, C. O. Avci, E. Grimaldi, C. Murer, J. Feng, M. Gabureac, C. Stamm, Y. Acremann, S. Finizio, S. Wintz, J. Raabe, and P. Gambardella, Spatially and time-resolved magnetization dynamics driven by spin-orbit torques, Nat. Nanotechnol. 12, 980 (2017).
- [26] Y. Kato, Y. Saito, H. Yoda, T. Inokuchi, S. Shirotori, N. Shimomura, S. Oikawa, A. Tiwari, M. Ishikawa, M. Shimizu, B. Altansargai, H. Sugiyama, K. Koi, Y. Ohsawa, and A. Kurobe, Improvement of write efficiency in voltage-controlled spintronic memory by development of a Ta-B spin Hall electrode, Phys. Rev. Appl. 10, 044011 (2018).
- [27] H. Honjo, T. V. A. Nguen, T. Watanabe, T. Nasuno, C. Zhang, T. Tanigawa, S. Miura, H. Inoue, M. Niwa, T. Yoshiduka, Y. Noguchi, M. Yasuhira, A. Tamakoshi, M. Natsui, Y. Ma, H. Koike, Y. Takahashi, K. Furuya, H. Shen, S. Fukami *et al.*, First demonstration of field-free SOT-MRAM with 0.35 ns write speed and 70 thermal stability under 400 °C thermal tolerance by canted SOT structure and its advanced patterning/SOT channel technology, 2019 IEEE International Electron Devices Meeting (IEDM), Francisco, CA (IEEE, 2019), p. 28.5.1.
- [28] Y. Saito, N. Tezuka, S. Ikeda, and T. Endoh, Antiferromagnetic interlayer exchange coupling and large spin Hall effect in multilayer systems with Pt/Ir/Pt and Pt/Ir layers, Phys. Rev. B 104, 064439 (2021).
- [29] Y. Saito, S. Ikeda, and T. Endoh, Synthetic antiferromagnetic layer based on Pt/Ru/Pt spacer layer with 1.05 nm interlayer exchange oscillation period for spin-orbit torque devices, Appl. Phys. Lett. 119, 142401 (2021).
- [30] Y. Saito, S. Ikeda, and T. Endoh, Enhancement of current to spin-current conversion and spin torque efficiencies in a synthetic antiferromagnetic layer based on a Pt/Ir/Pt spacer layer, Phys. Rev. B 105, 054421 (2022).
- [31] Y. Saito, S. Ikeda, and T. Endoh, Correlation between the magnitude of interlayer exchange coupling and charge-to-spin conversion efficiency in a synthetic antiferromagnetic system, Appl. Phys. Express 16, 013002 (2023).
- [32] Y. Saito, S. Ikeda, N. Tezuka, H. Inoue, and T. Endoh, Field-free spin-orbit torque switching and large dampinglike spin-orbit torque efficiency in synthetic antiferromagnetic systems using interfacial Dzyaloshinskii-Moriya interaction, Phys. Rev. B 108, 024419 (2023).
- [33] X. Qiu, K. Narayanapillai, Y. Wu, P. Deorani, D. H. Yang, W. S. Noh, J. H. Park, K. J. Lee, H. W. Lee, and H. Yang, Spin-orbit-torque engineering via oxygen manipulation, Nat. Nanotechnol. 10, 333 (2015).

- [34] H. An, Y. Kageyama, Y. Kanno, N. Enishi, and K. Ando, Spintorque generator engineered by natural oxidation of Cu, Nat. Commun. 7, 13069 (2016).
- [35] Y. Kageyama, Y. Tazaki, H. An, T. Harumoto, T. Gao, J. Shi, and K. Ando, Spin-orbit torque manipulated by fine-tuning of oxygen-induced orbital hybridization, Sci. Adv. 5, eaax4278 (2019).
- [36] G. Okano, M. Matsuo, Y. Ohnuma, S. Maekawa, and Y. Nozaki, Nonreciprocal spin current generation in surface-oxidized copper films, Phys. Rev. Lett. 122, 217701 (2019).
- [37] T. Gao, A. Qaiumzadeh, H. An, A. Musha, Y. Kageyama, J. Shi, and K. Ando, Intrinsic spin-orbit torque arising from the Berry curvature in a metallic-magnet/Cu-oxide interface, Phys. Rev. Lett. 121, 017202 (2018).
- [38] S. Q. Zheng, K. K. Meng, Q. B. Liu, Y. C. Wu, J. Miao, X. G. Xu, and Y. Jiang, Origin of large spin Hall magnetoresistance in Fe/CuO_x bilayers, Phys. Lett. A 384, 126198 (2020).
- [39] J. Kim, J. Uzuashi, M. Horio, T. Senoo, D. Go, D. Jo, T. Sumi, T. Wada, I. Matsuda, T. Ohkubo, S. Mitani, H.-W. Lee, and Y. C. Otani, Oxide layer dependent orbital torque efficiency in ferromagnet/Cu/oxide heterostructures, Phys. Rev. Mater. 7, L111401 (2023).
- [40] S. Ding, A. Ross, D. Go, L. Baldrati, Z. Ren, F. Freimuth, S. Becker, F. Kammerbauer, J. Yang, G. Jakob, Y. Mokrousov, and M. Kläui, Harnessing orbital-to-spin conversion of interfacial orbital currents for efficient spin-orbit torques, Phys. Rev. Lett. 125, 177201 (2020).
- [41] T. V. A. Nguyen, Y. Saito, H. Naganuma, D. Vu, S. Ikeda, and T. Endoh, Investigation of the dynamic magnetic properties in RuO₂/Co-Fe-B stack film, IEEE Trans. Magn. 60, 2200305 (2024).
- [42] Y. Saito, N. Tezuka, S. Ikeda, and T. Endoh, Spin Hall effect investigated by spin Hall magnetoresistance in Pt_{100-x}Au_x/CoFeB systems, AIP Adv. **9**, 125312 (2019).
- [43] See Supplemental Material at http://link.aps.org/supplemental/ 10.1103/PhysRevB.110.134423 for the x-ray diffraction (XRD) patterns in samples A–D; anomalous Hall effect (AHE) curves in samples A–D; estimated resistivity of Pt, [Pt/Ir] multilayer, Ru, Ti, and RuO₂; efficiency of effective field χ as a function of $H_{\rm ex}$ and dampinglike SOT efficiency $\xi_{\rm DL}$ as a function of $t_{\rm RuO_2}$ in sample E; magnitude of spin Hall conductivity ($\sigma_{\rm SH}$) as functions of $t_{\rm Pt}$, $t_{\rm PtIr}$, $t_{\rm Ru}$, and $t_{\rm Ti}$ for samples A–D; change in the R_{xy} under $H_x=0$ mT, after applying writing pulses for sample A ($t_{\rm Pt}=2.0$ nm); results of spin-torque ferromagnetic resonance (ST-FMR) measurement in sample F; and anomalous Hall effect (AHE) curves when an external magnetic field is applied in the in-plane direction in sample A. It also contains Refs. [30,31,42,45,46,48,54–61,64,69].
- [44] Y. Saito, N. Tezuka, S. Ikeda, H. Sato, and T. Endoh, Increase in spin-Hall effect and influence of anomalous Nernst effect on spin-Hall magnetoresistance in β -phase and α -phase W_{100-x}Ta_x/CoFeB systems, Appl. Phys. Express **12**, 053008 (2019).
- [45] R. Karplus and J. M. Luttinger, Hall effect in ferromagnetics, Phys. Rev. 95, 1154 (1954).
- [46] J. Smit, The spontaneous Hall effect in ferromagnetics I, Physica (Amsterdam) 21, 877 (1955).
- [47] S. Ikeda, K. Miura, H. Yamamoto, K. Mizunuma, H. D. Gan, M. Endo, S. Kanai, J. Hayakawa, F. Matsukura, and H. Ohno,

- A perpendicular-anisotropy CoFeB-MgO magnetic tunnel junction, Nat. Mater. 9, 721 (2010).
- [48] P. X. Zhang, L. Y. Liao, G. Y. Shi, R. Q. Zhang, H. Q. Wu, Y. Y. Wang, F. Pan, and C. Song, Spin-orbit torque in a completely compensated synthetic antiferromagnet, Phys. Rev. B 97, 214403 (2018).
- [49] T. Fache, J. C. Rojas-Sanchez, L. Badie, S. Mangin, and S. Petit-Watelot, Determination of spin Hall angle, spin mixing conductance, and spin diffusion length in CoFeB/Ir for spin-orbitronic devices, Phys Rev. B 102, 064425 (2020).
- [50] R. Ramaswamy, Y. Wang, M. Elyasi, M. Motapothula, T. Venkatesan, X. Qiu, and H. Yang, Extrinsic spin Hall effect in Cu_{1-x}Pt_x, Phys Rev. Appl. 8, 024034 (2017).
- [51] M. Isasa, E. Villamor, L. E. Hueso, M. Gradhand, and F. Casanova, Temperature dependence of spin diffusion length and spin Hall angle in Au and Pt, Phys Rev. B 91, 024402 (2015).
- [52] L. Wang, R. J. H. Wesselink, Y. Liu, Z. Yuan, K. Xia, and P. J. Kelly, Giant room temperature interface spin Hall and inverse spin Hall effects, Phys. Rev. Lett. 116, 196602 (2016).
- [53] H. Hayashi, D. Jo, D. Go, T. Gao, S. Haku, Y. Mokrousov, H.-W. Lee, and K. Ando, Observation of long-range orbital transport and giant orbital torque, Commun. Phys. 6, 32 (2023).
- [54] L. Han, Y. Wang, W. Zhu, R. Zhao, X. Chen, R. Su, Y. Zhou, H. Bai, Q. Wang, Y. Y., C. Chen, S. Yan, T. Chen, Y. Wen, C. Song, and F. Pan, Spin homojunction with high interfacial transparency for efficient spin-charge conversion, Sci. Adv. 8, eabq2742 (2022).
- [55] W. Zhang, W. Han, X. Jiang, S.-H. Yang, and S. S. P. Parkin, Role of transparency of platinum–ferromagnet interfaces in determining the intrinsic magnitude of the spin Hall effect, Nat. Phys. 11, 496 (2015).
- [56] L. Zhu, D. C. Ralph, and R. A. Buhrman, Highly efficient spin-current generation by the spin Hall effect in $Au_{1-x}Pt_x$, Phys. Rev. Appl. **10**, 031001 (2018).
- [57] L. Zhu, D. C. Ralph, and R. A. Buhrman, Effective spin-mixing conductance of heavy-metal-ferromagnet interfaces, Phys. Rev. Lett. 123, 057203 (2019).
- [58] L. Liu, T. Moriyama, D. C. Ralph, and R. A. Buhrman, Spintorque ferromagnetic resonance induced by the spin Hall effect, Phys. Rev. Lett. 106, 036601 (2011).
- [59] D. Fang, H. Kurebayashi, J. Wunderlich, K. Výborný, L. P. Zârbo, R. P. Campion, A. Casiraghi, B. L. Gallagher, T. Jungwirth, and A. J. Ferguson, Spin-orbit-driven ferromagnetic resonance, Nat. Nanotechnol. 6, 413 (2011).
- [60] T. Nan, C. X. Quintela, J. Irwin, G. Gurung, D. F. Shao, J. Gibbons, N. Campbell, K. Song, S.-Y. Choi, L. Guo, R. D. Johnson, P. Manuel, R. V. Chopdekar, I. Hallsteinsen, T. Tybell, P. J. Ryan, J.-W. Kim, Y. Choi, P. G. Radaelli, D. C. Ralph *et al.*, Controlling spin current polarization through non-collinear antiferromagnetism, Nat. Commun. 11, 4671 (2020).
- [61] D. MacNeill, G. M. Stiehl, M. H. D. Guimaraes, R. A. Buhrman, J. Park, and D. C. Ralph, Control of spin-orbit torques through crystal symmetry in WTe₂/ferromagnet bilayers, Nat. Phys. 13, 300 (2017).
- [62] A. Fert, V. Cros, and J. Sampaio, Skyrmions on the track, Nat. Nanotechnol. **8**, 152 (2013).
- [63] S.-H. Yang, K.-S. Ryu, and S. Parkin, Domain-wall velocities of up to 750 ms⁻¹ driven by exchange-coupling torque in synthetic antiferromagnets, Nat. Nanotechnol. 10, 221 (2015).

- [64] S. Fukami, C. Zhang, S. DuttaGupta, A. Kurenkov, and H. Ohno, Magnetization switching by spin-orbit torque in an antiferromagnet-ferromagnet bilayer system, Nat. Mater. 15, 535 (2016).
- [65] L. Zhu, K. Sobotkiewich, X. Ma, X. Li, D. C. Ralph, and R. A. Buhrman, Strong damping-like spin-orbit torque and tunable Dzyaloshinskii–Moriya interaction generated by low-resistivity Pd_{1-x}Pt_x alloys, Adv. Funct. Mater. 29, 1805822 (2019).
- [66] C.-Y. Hu and C.-F. Pai, Benchmarking of spin-orbit torque switching efficiency in Pt alloys, Adv. Quantum Technol. 3, 2000024 (2020).
- [67] M.-H. Nguyen, M. Zhao, D. C. Ralph, and R. A. Buhrman, Enhanced spin Hall torque efficiency in $Pt_{100-x}Al_x$ and $Pt_{100-x}Hf_x$ alloys arising from the intrinsic spin Hall effect, Appl. Phys. Lett. **108**, 242407 (2016).
- [68] C.-Y. Hu, Y.-F. Chiu, C.-C. Tsai, C.-C. Huang, K.-H. Chen, C.-W. Peng, C.-M. Lee, M.-Y. Song, Y.-L. Huang, S.-J. Lin, and C.-F. Pai, Toward 100% spin—orbit torque efficiency with high spin—orbital Hall conductivity Pt–Cr alloys, ACS Appl. Electron. Mater. 4, 1099 (2022).
- [69] P. Fan, K. Yi, J.-D. Shao, and A.-X. Fan, Electrical transport in metallic films, J. Appl. Phys. **95**, 2527 (2004).